Adsorption of arsenic(V) onto single sheet iron oxide: X-ray absorption fine structure and surface complexation

Zhou Yin [a,*], Johannes Lützenkirchen [b], Nicolas Finck [b], Noémie Celaries [c], Kathy Dardenne [b], Hans Chr. Bruun Hansen [a]

[a] *Dept. of Plant and Environmental Sciences, University of Copenhagen, Denmark*
[b] *Institut für Nukleare Entsorgung (INE), Karlsruher Institut für Technologie (KIT), Karlsruhe, Germany*
[c] *Institut de Chimie Moléculaire de Reims (ICMR), Reims, France*[1]

GRAPHICAL ABSTRACT

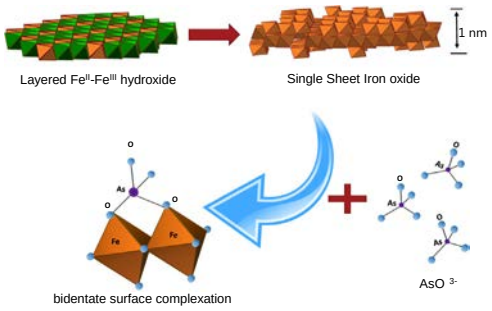

ARTICLE INFO

Keywords:
Single sheet iron oxide
Delamination
Arsenate
Surface complexation
Basic stern model

ABSTRACT

Adsorption onto two dimensional nanosheet materials offers new possibilities for fast and efficient removal of contaminants from waters. Here, the adsorption of As(V) to a new type of iron oxides single sheet iron oxide (SSI) has been studied as a function of time, loading and pH. Adsorption of As(V) onto SSI was very fast compared to other iron oxides, with 80% of total As(V) adsorbed within 10 min. Examination by extended X ray absorption fine structure analysis showed that As(V) forms a bidentate inner sphere surface complex with SSI. Arsenic(V) adsorption isotherms and adsorption envelopes were well described using a 1 pK Basic Stern surface complexation model involving protonated ($\equiv Fe_2O_2AsO_2H$) and unprotonated ($\equiv Fe_2O_2AsO_2^{2}$) inner sphere surface complexes. The surface com plexation constants for As(V) binding to SSI is similar to constants found for goethite and ferrihydrite. Simulated adsorption isotherms for intermediate As(V) concentrations also demonstrate that SSI is per forming equally well as goethite and ferrihydrite based on surface area normalized adsorption capacities. The binding affinities at micromolar to submicromolar As(V) solution concentrations are similar for SSI and ferrihydrite. SSI has interesting potential as a stable, high affinity sorbent for use in applications where efficient and fast removal is required.

1. Introduction

Arsenic contamination of natural waters is a global problem due to industrial waste discharge, agricultural use of pesticides and geologic contamination. Exposure to inorganic arsenic affects blood vessels, kidney, liver, lungs and skin, leading to the

* Corresponding author.
E-mail addresses: yin@plen.ku.dk (Z. Yin), johannes.luetzenkirchen@kit.edu (J. Lützenkirchen), nicolas.finck@kit.edu (N. Finck), noemie.celaries@univ-reims.fr (N. Celaries), kathy.dardenne@kit.edu (K. Dardenne), haha@plen.ku.dk (H.C.B. Hansen).
[1] Previous address: Ecole Nationale Supérieure de Chimie de Rennes, France.

significant toxicity of arsenic to humans [1]. Arsenic is often pre sent in groundwater dominated by trivalent As(III) under anaero bic conditions and pentavalent As(V) under aerobic conditions [2]. According to the World Health Organization (WHO), the threshold concentration of arsenic in drinking water is 10 μg/L [3]. Therefore, major efforts are made to develop efficient sorbents with high affinity for arsenic removal in drinking and irrigation water.

Many materials have been used to remove arsenic from aque ous solutions by adsorption, such as Fe^{III} (hydr)oxides, zeolites, active carbon, anionic clays, etc. Among these sorbents, Fe^{III} (hydr)oxides have attracted special attention due to their strong interaction with arsenic and their large adsorption capacities. Thus, numerous studies have investigated arsenic adsorption on Fe^{III} (hydr)oxides, such as ferrihydrite, goethite, feroxyhyte and hema tite [4 9]. Arsenic binding properties of those Fe^{III} (hydr)oxides are strongly determined by the structure of the particle surface and the type of surface complexes formed. Various *in situ* techniques such as X ray absorption spectroscopy and infrared spectroscopy have been used for surface speciation. In addition to these techniques, surface complexation modelling (SCM) is a powerful tool to quan tify surface speciation and trace changes depending on conditions such as pH, electrolyte, concentration, sorbent loading, competing sorbates, etc. [10]. A number of surface complexation models which differ in complexity have been applied to describe the uptake mechanism for As(V) on Fe^{III} (hydr)oxides, including the Constant Capacitance Model (CCM) [11], the Diffuse Layer Model (DLM) [12,13], the Basic Stern Model (BSM) [14,15] and the Three Plane Model (TPM) involving Charge Diffusion and Multi Site Complexation (CD MUSIC) options [16 18]. The DLM has been widely applied to various types of Fe^{III} (hydr)oxides [12,19,20], while the TPM implemented in the CD MUSIC Model originally developed for Fe^{III} (hydr)oxides with regular surfaces like goethite [16 18], is now also successfully applied for less crystalline Fe^{III} (hydr)oxides like ferrihydrite [21,22]. DLM, CCM and TPM have tra ditionally adopted the so called 2 pK approach proposed by Parks [23], in which the protonation of the surface OH groups is described in two steps. The 1 pK approach with only one protona tion step in the accessible pH range has often been applied in com bination with the BSM [24]. One major advantage of the 1 pK model compared to the 2 pK model is a reduction in the number of adjustable parameters.

Recently, the successful preparation of a two dimensional (2D) single layered nanosheet material by delamination of layered dou ble hydroxides (LDHs) has opened a new pathway to obtain nanosheets with a high specific surface area [25 28]. These 2D materials may be ideal as sorbents, catalysts, capacitors, and carri ers in drug delivery. Previous studies have shown that the adsorp tion capacity of LDHs is notably determined by the composition and the properties of the metal hydroxide layers [29,30]. Therefore, by combining the advantages of delaminated LDHs and the high bind ing affinity of metal (hydr)oxides, a strong, fast reacting and high capacity arsenic sorbent may be formed. Here, such a new type of 2D Fe^{III} (hydr)oxides termed Single Sheet Iron oxide (SSI) has been prepared by oxidation of Fe^{II} Fe^{III} LDHs (Green Rust, GR). In our pre vious work, we have demonstrated how to synthesize SSIs, starting from dodecanoate intercalated GR, followed by solid state oxida tion with oxygen and delamination in alkaline solutions [31 33]. Compared to other Fe^{III} (hydr)oxide particles, SSI with a thickness of 1 nm and lateral dimensions varying from 20 to 100 nm, has the highest surface area to volume ratio possible, ideally with all Fe OH groups exposed to the solution. In SSI, the brucite type Fe^{III} (hydr)oxide layer of GR is altered via vertical displacement of Fe atoms from the original hydroxide layer to form a trilayer structure with Fe polyhedra linked via both corner and edge sharing [33]. Therefore, SSI has a higher density of singly or doubly coordinated hydroxyl groups compared to the parent metal hydroxide layers in GR where only triply coordinated hydroxyl groups are present on planar surfaces (Fig. 1) [33]. In addition, the high specific surface area and full exposure of all reactive sites make SSI an interesting sorbent for species that bind via surface complexation.

With the altered brucite layer structure and the ultrathin thick ness, it is hypothesized that SSI will permit fast sorption and strong binding of As(V). In this work, SSI was prepared for studies of As(V) adsorption from aqueous solutions. We have characterized As(V) binding to the SSI particle surfaces using X ray absorption near edge structure (XANES) and X Ray Absorption Fine Structure (EXAFS). Potentiometric titration of SSI has been performed to derive surface complexation equilibrium constants for protonation, deprotonation and interaction with electrolyte ions by using the 1 pK BSM. Data for adsorption kinetics, isotherms at constant pH and adsorption as a function of pH has been obtained. With these data and the spectroscopic identification of As(V) surface species, we have derived surface complexation equilibrium constants for As (V) binding to SSI.

2. Experimental section

2.1. Materials

The synthesis of SSI was carried out as described by Yin *et al.* [33]. In short, the preparation was started by synthesis of the chlo ride form of GR (GR_{Cl}) and exchanging chloride with dodecanoate, followed by solid state oxidation with oxygen, delamination under alkaline conditions, and final removal of dodecanoate and washing. A concentrated SSI suspension was used as sorbent stock suspen sion. The concentration of SSI in the stock suspension was deter mined by triplicate measurements of the mass of SSI in 0.5 mL solution by drying on an aluminum foil at 60 °C overnight. The specific surface area of washed and freeze dried SSI was deter mined by N_2 gas adsorption using the BET method [34] with a Micromeritics Gemini VII instrument. The sample was degassed at 40 °C for 12 h under a continuous stream of dry N_2 prior to BET measurement. A specific surface area of SSI of 237 ± 7 m^2/g was determined. A stock solution of 2.67 mmol/L (200 mg/L) As (V) was prepared from Na_2HAsO_4 $7H_2O$ (Fluka, 98%). Sodium nitrate ($NaNO_3$, ≥99%), sodium hydroxide (NaOH, 98%), and nitric acid (HNO_3, 70%) were all obtained from Sigma Aldrich. All solu tions and suspensions were prepared by weight, and dilutions made using ultrapure water (18.2 MΩ cm, Milli Q system, Millipore).

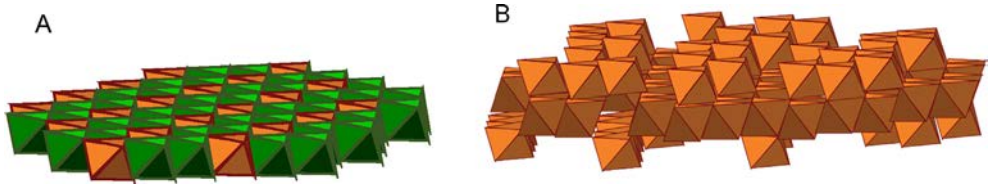

Fig. 1. The structure of (A) a Fe^{II}-Fe^{III} hydroxide layer of Green Rust; (B) Single Sheet Iron oxide derived from Green Rust (green octahedra contain Fe^{II} and brown octahedra Fe^{III} [33].

2.2. Acid base titrations

The point of zero charge of SSI was determined from the cross over point of potentiometric titrations as described by Lützen kirchen *et al.* [35]. Briefly, a volume of 5 mL of a 30 g/L SSI stock suspension was diluted to obtain 50 mL of a 3 g/L SSI suspension with $NaNO_3$ as background electrolyte at three concentrations of 1 mmol/L, 10 mmol/L and 100 mmol/L. Titrations were conducted in an airtight vessel with argon (purity > 99.99%) bubbled through the suspension at a flow of 35 mL/min to minimize CO_2 intrusion. The argon used was passed through washing bottles of acid (HNO_3, 0.1 mol/L), base (NaOH, 0.1 mol/L) and background electrolyte solution before being introduced in the titration vessel. The sus pension was equilibrated over night (>8h) in an argon atmosphere under gentle stirring (50 rpm). Pre equilibration was done at pH around 10 by adjustment with 0.01 mol/L NaOH. The titration was done by adding 0.2 mL of 0.01 mol/L HNO_3 per step with two minutes waiting time between additions. The pH electrode (Metrohm) was calibrated with buffer solutions at pH 4.0, 7.0 and 9.4. The surface charge density was calculated by:

$$\sigma \quad \frac{F}{sy}(C_A \quad C_B \quad [H^+] + [OH^-]) \tag{1}$$

where σ is the surface charge density of SSI (C/m^2), *F* is the Faraday constant (C/mol), *s* is the specific surface area of SSI (m^2/g), *y* is the mass concentration of SSI (g/L), C_A and C_B are the concentrations of acid or base added to the suspension (M), and $[H^+]$ and $[OH^-]$ are the concentrations (mol/L) of H^+ and OH^- determined from the pH of the suspension.

2.3. Adsorption kinetics

The rate of arsenic adsorption to SSI was studied by batch experiments with varying reaction times in 100 mL polyethylene beakers. Arsenic adsorption was studied as a function of pH (4.0, 7.0, 9.4), and at 11 different contact times with a maximum of 360 min. For each pH, an SSI suspension (0.2 g/L) with a back ground electrolyte of 0.01 mol/L $NaNO_3$ and an As(V) initial con centration of 267 μmol/L was used. The pH of the supernatants was maintained using 0.1 mol/L HNO_3 or NaOH as titrants while stirring with a Teflon coated magnetic bar (300 rpm). The sampled suspension was passed through a membrane filter (0.25 μm pore size, regenerated cellulose membrane filter, Mikrolab Aarhus A/S) before As determination in the filtrates. Iron in the filtrates after fil tration was measured after acidification by Atomic Absorption Spectroscopy (PerkinElmer FAAS PinAAcle 900F) showing concen trations of less than 0.1 mg/L corresponding to less than 5‰ of the total Fe concentration in the SSI. Therefore, almost all SSI was retained on the filter, and the minute amount of SSI passing through the filter was neglected. Duplicates were carried out for each experiment.

Arsenic(V) analysis was performed using graphite furnace atomic absorption spectroscopy (GFAAS, PerkinElmer PinAAcle 900Z), with an electrodeless discharge lamp (EDL) as the radiation source (wavelength: 193.7 nm). The detection limit was 0.05 μg/L, and the quantification limit was 0.16 μg/L. Kinetic data were fitted by non linear regression using Origin Pro 9.1. The adsorption kinetics may be modelled using a pseudo second order model [36]. Eq. (2) expresses the rate of As(V) adsorption on SSI:

$$dq_t/dt \quad k_2(q_e \quad q_t)^2 \tag{2}$$

where k_2 is the pseudo second order rate constant ($m^2/(\mu mol\ min)$), q_e is the amount of As(V) adsorbed (μmol/ m^2) at equilibrium and q_t is the amount of As(V) adsorption (μmol/ m^2) at time t.

In order to simplify the fitting, Eq. (2) is reduced to (Supplemen tal Information):

$$q_t \quad \frac{ABt}{1+At} \tag{3}$$

where *A* is $k_2 q_e$, and *B* is q_e (see also Supplemental Information).

2.4. Adsorption isotherms

Adsorption isotherms were obtained by batch experiments with varying As(V) concentrations in 50 mL polyethylene centrifuge tubes. Experiments were carried out at pH 4.0, 7.0, and 9.4 at 13 initial As(V) solution concentrations of 0 (as a blank), 2.67, 5.34, 8.01, 10.7, 13.4, 26.7, 53.4, 80.1, 106.8, 133.5, 200.3, and 267.1 μmol/L (corresponding to 0, 0.2 ,0.4, 0.6, 0.8, 1, 2, 4, 6, 8, 10, 15, and 20 mg As/L), SSI concentration of 0.2 g/L, and back ground electrolyte of 0.01 mol/L $NaNO_3$. Equilibration time was set to 360 min based on the kinetic adsorption study described above. The pH was kept constant by addition of 0.1 mol/L HNO_3 or NaOH at 4.0, 7.0, or 9.4 for the first 60 min, as preliminary exper iments showed that most of the adsorption reaction was complete after this time, and thus the pH drift was minimal after that. There after, the centrifuge tubes were capped and shaken at 240 rpm on a reciprocating shaker. The pH of the suspension was readjusted every 60 min. On termination, the suspensions were filtered using 0.25 μm membrane filters for separation and As determined in the filtrates using GFAAS as described above.

2.5. Adsorption envelopes

The influence of pH on As(V) adsorption was investigated in the pH range from 3.5 to 9.5. The experimental setup was the same as for the adsorption isotherm experiments, except for the concentra tion of As(V) which was kept constant, at two initial concentrations of 1.33 and 267.1 μmol/L (corresponding to 0.1 and 20 mg As/L), respectively. The pH of the suspensions was adjusted using 0.1 mol/L HNO_3 or NaOH. After setting the pH, the centrifugation tubes were capped and shaken at 240 rpm on a reciprocating sha ker for 3 h, followed by membrane filtering of the supernatant and As determination by GFAAS as described above.

2.6. X ray absorption spectroscopy

Molecular scale information on the structure of surfaces com plexes was obtained by X ray absorption spectroscopy (XAS) at the As *K* edge. XAS spectra were recorded at the INE beamline [37] at the Karlsruhe Institute of Technology Synchrotron Light Source (Karlsruhe, Germany) with a storage ring energy of 2.5 GeV. The beam energy was calibrated by assigning the first inflection point of the L_3 edge XANES recorded from an Au foil measured in parallel to 11918 eV. Data were recorded in fluores cence mode at room temperature using a silicon drift detector (Vortex ME4, Hitachi). For each sample, 3 4 scans were collected to achieve an adequate signal to noise ratio. XAS samples were prepared using 20 g/L SSI, 0.01 mol/L $NaNO_3$, and 27 mmol/L initial As(V) concentration with different pH (4.0, 7.0 and 9.4). After equi libration, the suspensions were centrifuged at 6000 *g* for 3 min, and the sediment separated and washed with water. The wet paste was collected for XAS analysis. Athena (v. 0.9.25) and Artemis (v. 0.9.25) interfaces to the IFEFFIT software were used to analyze XAS data following standard procedures [38]. EXAFS spectra were extracted from the raw data and Fourier transforms were obtained from the $k^3 \times \chi(k)$ functions using a Kaiser Bessel window. Final fitting of the spectra was done using phase and amplitude func tions calculated with FEFF6 in R space [39]. Plausible adsorption structures are based on the SSI face structure and bond distances

inferred from preliminary Pair Distribution Function fits [33]. Coordination number (N), energy shift (ΔE_0), adjustment to interatomic distance (ΔR), and the Debye Waller parameter (σ^2) were treated as fitting parameters for each shell, while the amplitude reduction factor ($S_0^2 = 1$) was determined according to the fitting of the reference compound (aqueous As(V) solution without SSI). The model was adjusted shell by shell to the Fourier transform of the k^2 and k^3 weighted spectra. In agreement with Sherman and Randall [45] multiple scattering involving O—O pairs within the AsO_4 tetrahedron was included in the fitting procedure. The fit quality was quantified by the R_f factor representing the absolute misfit between theory and data.

2.7. Surface complexation modelling

In this work, a 1 pK BSM was employed to describe the acid base titration and the As(V) adsorption data, for two reasons: (i) it simplifies salt concentration effects into a single set of model parameters, and (ii) it provides a better and more comprehensive description of the surface charge of SSI based on the potentiometric titration data compared to other surface complexation models (e.g. CCM or DLM). Besides, the 1 pK BSM model has provided excellent fits for proton titration data for other Fe^{III} (hydr)oxides [40,41]. To derive acid base surface complexation constants and ion pairing constants for electrolyte ions (e.g. Na^+ and NO_3^-) based on the potentiometric titrations, a modified version of FITEQL [42] coupled to UCODE [43] was used. With this approach, the surface complexation constants and the capacitance value could be estimated through a least square fitting for all electrolyte concentrations simultaneously. The 1 pK model assumes that the protonated surface oxygen may have fractional values of charge. The singly, doubly and triply coordinated OH groups of the SSI surface are here denoted as $\equiv FeOH^{-1/2}$, $\equiv Fe_2OH^0$, $\equiv Fe_3O^{-1/2}$, where the −1/2 and 0 values represent the formal charges of the respective groups. This charge is deduced by applying Pauling's rule to Fe and O atoms in the surface [44,45]. SSI structures and surfaces were studied in previous work [33], in which the surface site densities obtained for singly, doubly, and triply coordinated OH groups were estimated to 5.2 sites/nm^2, 6.5 sites/nm^2, and 4 sites/nm^2, respectively. Previous studies of As(V) adsorption to Fe^{III} (hydr)oxides have shown that As(V) mainly binds as inner sphere bidentate complexes with singly coordinated surface OH groups [46–48]. Based on a combination of EXAFS and IR spectroscopy for As(V) adsorption on goethite, it was concluded that As(V) coordinates predominantly to singly coordinated OH groups on the goethite surface where it is stabilized by hydrogen bonding to neighboring surface sites. Singly coordinated OH have been identified as most important for metal ion sorption in ferrihydrite systems as well [49,50]. However, Loring *et al.* questioned previous conclusions [51], and claimed that the As Fe distance on goethite does not match to the "generally accepted" structure. For SSI, the structural arrangement of the different OH groups is not as clear as for goethite. Based on the previous studies, we have chosen a pragmatic approach restricting As(V) sorption to singly, doubly and triply coordinated OH groups. The affinity of the background electrolyte ions to the singly and triply coordinated sites required for a good fit turned out to be rather weak. The association constant was fixed to a common value for both anions and cations on the singly and triply coordinated groups. The doubly coordinated group has been reported with strong cation association earlier [52], and was therefore assumed to be different. Proton affinity constants and site densities were *a priori* fixed, using previously published value for the latter. The proton affinity of the singly and triply coordinated groups was fixed at the point of zero charge, while the values for the doubly coordinated group were assumed to be similar to those on goethite [53]. Including the weak association constant in the number of parameters, we finally fitted a total of 3 adjustable parameters (two association constants and the capacitance value).

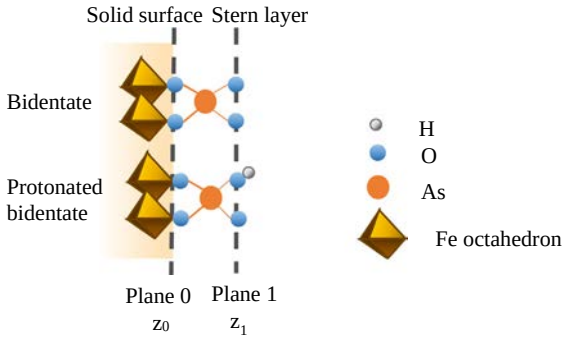

Fig. 2. Schematic drawing of the SSI water interface showing two different hypothetical inner-sphere As(V) surface complexes. Electrolyte ions, Na^+ and NO_3^-, are not shown, but are located in plane 1, and are present as outer-sphere complexes.

To derive and optimize As(V) surface complexation constants for SSI, Visual MINTEQ [54] coupled with PEST [55] was used. Based on the conclusions from the EXAFS investigation, two different types of As(V) SSI surface complexes (non protonated bidentate and protonated bidentate) were tested in this fitting exercise, as shown in Fig. 2. In the model, the charge distribution values (Δz_0 and Δz_1) for the bidentate As(V) surface complexes were calculated assuming −3/4 charge units per As(V) oxygen (Fig. 2). As shown in Table 2, two Fe—O—As bonds with the SSI surface require a change in charge of −1.5, and the co adsorption of 2 protons to release two water molecules, resulting in a change of +0.5 in the surface ("0") plane. This leaves −1.5 for the head end of the diffuse layer (Eqs. (4a) and (4b)).

$$\Delta z_0 \quad 2 \times \frac{3}{4} + 2 \tag{4a}$$

$$\Delta z_1 \quad 2 \times \frac{3}{4} \tag{4b}$$

For the protonated bidentate species the extra proton is accordingly taken into account. Therefore, $\Delta z_0 = 0.5$ and $\Delta z_1 = 0.5$ are obtained implying that the extra proton goes to plane 1. This assignment results in the best fits.

3. Results and discussions

3.1. Acid base titration of SSI

The interfacial electrostatic charge of the SSI particle due to protonation obtained by potentiometric titration of SSI suspensions at the three different electrolyte concentrations is shown in Fig. 3. As seen from the cross over of the titration curves, the point of zero net proton charge is 7.8. Around this pH, the measured charging curves flatten, which is usually observed at the point of zero charge at sufficiently low salt concentrations. The isoelectric point (IEP) of the dried powder was measured and found to occur at around pH 7.8, i.e. close to the observed point of zero net proton charge (data not shown). The previous measurement of the IEP of SSI yielded a higher value of around pH 9.2 [32]. However, in that study titration was commenced at pH around 3 which may have caused partial SSI dissolution. The re adsorption of dissolved Fe^{III} increased the IEP, similar to what has been observed for aluminum oxides [56]. This problem is circumvented in the present study and thus the point of zero net proton charge around 7.8 is regarded as a reliable estimate.

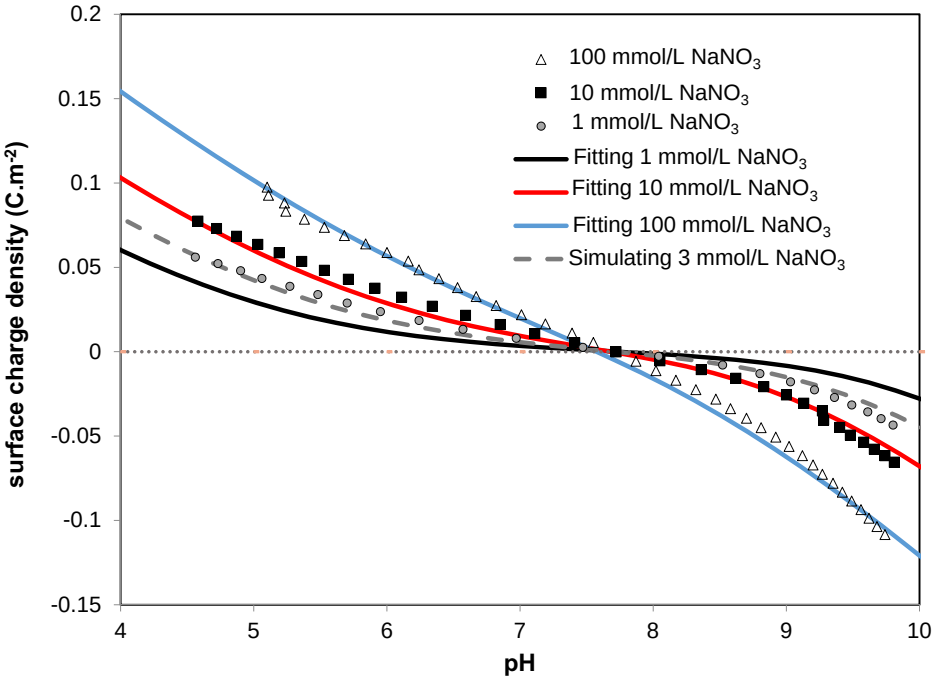

Fig. 3. Surface protonation dependent charge density determined from potentiometric titrations of SSI suspensions at three electrolyte concentrations. Triangle, square and circle spots are experimental data, while colored curves represent simulations by the 1-pK BSM.

In the model, the equations and the surface complexation constants for protonation, deprotonation and surface complexation of $\equiv FeOH^{1/2}$, $\equiv Fe_2OH^0$, and $\equiv Fe_3O^{1/2}$ groups with the electrolyte ions are listed in Table 1. The protonation equilibria reflect that at high pH, the surface is mainly populated with $\equiv FeOH^{1/2}$, $\equiv Fe_2O^{1}$, and $\equiv Fe_3O^{1/2}$ groups, resulting in a net negative surface charge. At low pH, the surface is mainly populated with $\equiv FeOH^{+1/2}$, $\equiv Fe_2OH_2^{+}$, and $\equiv Fe_3OH^{+1/2}$ groups, resulting in a net positive surface charge. Generally, the modelled curves describe the data reasonably well, except at low $NaNO_3$ concentration (1 mmol/L) (Fig. 3). The misfit at low $NaNO_3$ concentration may be due to a high concentration of SSI (3 g/L) requiring considerable quantities of HNO_3 or NaOH for pH adjustment, which enhances the effective ionic strength and thus the measured charge. Using the final model with an electrolyte concentration of 3 mmol/L yields a very good description of the nominal 1 mmol/L data. The Stern layer capacitance C_{stern} is estimated to 1.47F/m^2 by the fitting, which is in the range of published values [57].

3.2. Kinetics of As(V) adsorption on SSI

The kinetics of As(V) adsorption by SSI at three pH values is shown in Fig. 4. With increasing pH, the adsorbed amount of As (V) decreases from 3.22 μmol/m^2 (pH 4) to 1.30 μmol/m^2 (pH 9.4). The rate of As(V) adsorption may be divided into three stages. In the first stage up to 10 min, As(V) adsorption (q_t) rapidly increases with time. In the second stage between 10 and 60 min, q_t slowly increases with time. In the final stage at 60 min, where q_t stays constant, the equilibrium is reached. As(V) adsorption is fast with rate constants ranging from 0.06 to 0.19 m^2/(μmol) min, fastest at low pH. Table 2 summarizes the calculated q_e and k_2 values for the second order model (Eq. (2)).

3.3. X ray absorption spectroscopy

The normalized XANES spectra of the As(V)(aq) reference sample and SSI with adsorbed As(V) are shown in Fig. 5. XANES

Table 1
Surface complexes, and the corresponding surface complexation reactions and intrinsic surface complexation constants estimated from acid-base titration of SSI and application of the 1-pK BSM model.

Surface species	Δz_0[a]	Δz_1[b]	Reaction	log K
$\equiv FeOH_2^{+1/2}$	1	0	$\equiv FeOH^{1/2} + H^+ \rightleftharpoons \equiv FeOH_2^{+1/2}$	7.77[d]
$\equiv FeOH^{1/2}\cdots Na^+$	0	1	$\equiv FeOH^{1/2} + Na^+ \rightleftharpoons \equiv FeOH^{1/2}\cdots Na^+$	< −2.8[e]
$\equiv FeOH_2^{+1/2}NO_3$	0	−1	$\equiv FeOH_2^{+1/2} + NO_3 \rightleftharpoons \equiv FeOH_2^{+1/2}\cdots NO_3$	< −2.8[e]
$\equiv Fe_2OH_2^{+}$	1	0	$\equiv Fe_2OH^0 + H^+ \rightleftharpoons \equiv Fe_2OH_2^{+}$	0.15[c]
$\equiv Fe_2O$	−1	0	$\equiv Fe_2OH^0 \rightleftharpoons \equiv Fe_2O + H^+$	−11.5[c]
$\equiv Fe_2O^{1}\cdots Na^+$	−1	1	$\equiv Fe_2OH^0 + Na^+ \rightleftharpoons \equiv Fe_2O^{1}\cdots Na^+ + H^+$	−8.57
$\equiv Fe_2OH_2^{+1}NO_3$	0	−1	$\equiv Fe_2OH_2^{+} + NO_3 \rightleftharpoons \equiv Fe_2OH_2^{+1}NO_3$	< −2.8[e]
$\equiv Fe_3OH^{+1/2}$	1	0	$\equiv Fe_3O^{1/2} + H^+ \rightleftharpoons \equiv Fe_3OH^{+1/2}$	7.77[d]
$\equiv Fe_3O^{1/2}\cdots Na^+$	0	1	$\equiv Fe_3O^{1/2} + Na^+ \rightleftharpoons \equiv Fe_3O^{1/2}\cdots Na^+$	< −2.8[e]
$\equiv Fe_3OH^{+1/2}\cdots NO_3$	0	−1	$\equiv Fe_3OH^{+1/2} + NO_3 \rightleftharpoons \equiv Fe_3OH^{+1/2}\cdots NO_3$	< −2.8[e]

[a] The charge distribution values of plane 0.
[b] The charge distribution values of plane 1 (Fig. 2).
[c] Fixed.
[d] Fixed at PZC.
[e] log K were constrained to identical parameter values during fitting.

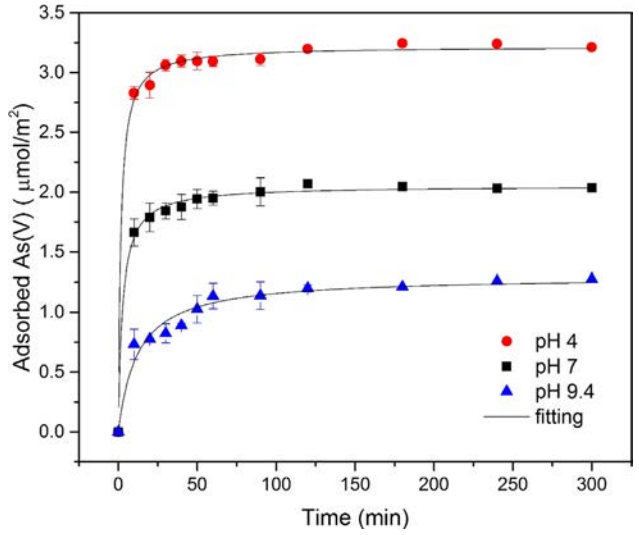

Fig. 4. Arsenic(V) adsorption kinetics to SSI at pH 4.0, 7.0, and 9.4 with fits to pseudo-second-order rate equation (Eq. (4)). (Initial As(V) concentration 270 μmol/L, SSI dose = 0.2 g/L, background electrolyte 0.01 mol/L $NaNO_3$). Error bars represent the difference between each duplicate.

Table 2
Pseudo-second-order rate constants for As(V) adsorption by SSI (Eq. (2)).

pH	q_e μmol/m²	k_2 m²/(μmol min)	R^2
4.0	3.22 (±0.01)[a]	0.19 (±0.02)	0.9975
7.0	2.05 (±0.01)	0.18 (±0.02)	0.9967
9.4	1.30 (±0.03)	0.06 (±0.01)	0.9620

[a] Uncertainty estimate is shown in the parentheses.

of sorption samples are located at similar energy position as the As (V)(aq) reference compound, but show features that are slightly different from the As(V)(aq) sample. The oxidation state of As did not change upon surface sorption, but XANES spectra hint at a modification of the first ligand sphere and exchange of water mole cules for the SSI surface ligands after sorption. For the sorption samples, there are no significant differences between pH 4 and 7 while there is a tiny difference for the XANES at pH 9.4, suggesting similar coordination geometry for pH 4 and 7, and small changes in sorption species at pH 9.4.

Fits to the EXAFS data provide information on the molecular structure of surface species. Experimental and modeled EXAFS spectra with the corresponding Fourier Transforms (FT) of As(V) adsorbed SSI and As(V)(aq) samples are displayed in Fig. 5 and structural parameters obtained from the linear least square fits of the EXAFS data are shown in Table 3. The EXAFS spectrum of the As(V)(aq) reference compound displays a single wave fre quency with monotonically decreasing amplitude and was mod eled considering a single O shell located at $R_{As\text{-}O1}$ = 1.69(2) Å and containing 4 atoms. The EXAFS spectra of the sorption samples dif fer from that of the As(V)(aq) sample, mainly with respect to the amplitude of the oscillations at k > 6 Å ^{1}, and the features at e.g., k ∼ 5 and 10.5 Å ^{1}. These findings provide clear indications that the As(V) molecular environment changed upon contact with SSI in suspension, and this agrees with XANES data. For all As(V) SSI samples, the first FT contribution was fit with 4 oxygen atoms at 1.70 Å. Coordination number and bond distance correspond to the regular AsO_4 tetrahedron, with As—O distances ranging from 1.68 to 1.70 Å (e.g. Loye *et al.* [58]), and agree with reported XAS data for As(V) adsorbed to other mineral surfaces [59]. The FT of the sorption samples further contain a broad contribution centered around ∼3 Å (not corrected for phase shift). A good fit to the data was obtained considering an Fe shell at $R_{As\text{-}Fe}$ = 3.27 3.28 Å and

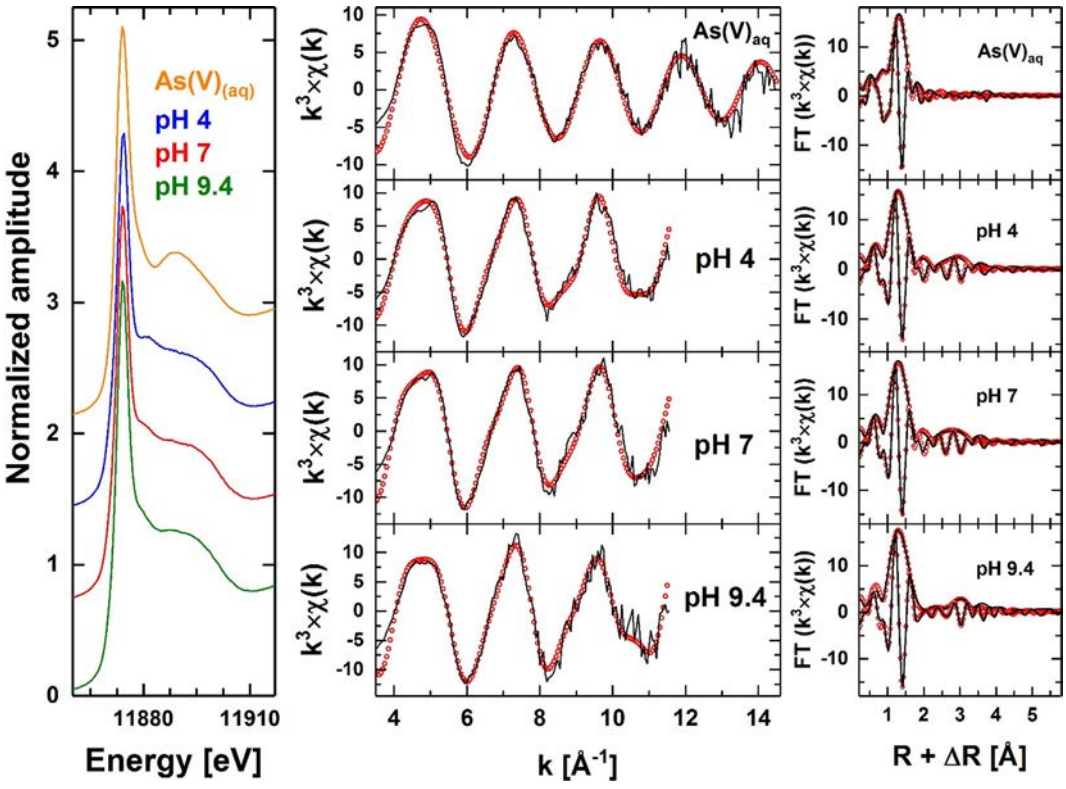

Fig. 5. XANES (left panel), experimental (solid black line) and modeled (red dots) EXAFS spectra (middle panel) with the corresponding Fourier transforms (right panel) of the As(V)(aq) and As(V)-SSI samples (27 mmol/L initial As(V) solution concentration, SSI dose 20 g/L, background electrolyte 0.01 mol/L $NaNO_3$). Fit results are presented in Table 3.

Table 3
Best fit EXAFS model parameters for As(V)(aq) reference compound ([As(V)] = 27 mmol/L without SSI) and the As(V)-SSI sorption samples.

	As(V)(aq)			pH 4			pH 7			pH 9.4		
Δk [Å ^{1}]	4.5–13.0			4.5–11.0			4.5–11.0			4.5–10.9		
ΔR [Å]	1.1–2.2			1.0–3.3			1.0–3.3			1.0–3.3		
R_f	0.006			0.012			0.012			0.003		
ΔE [eV]	6			O shell: 8 Fe shell: −9			O shell: 8 Fe shell: −9			O shells: 9 Fe shell: −9		
Shell	**N**	**R [Å]**	**σ^2 [Å^2]**	**N**	**R [Å]**	**σ^2 [Å^2]**	**N**	**R [Å]**	**σ^2 [Å^2]**	**N**	**R [Å]**	**σ^2 [Å^2]**
O1	4.0	1.69(2)	0.003	4.0	1.70(2)	0.002	4.0	1.70(2)	0.001	4.0	1.70(2)	0.001
O2	/	/	/	/	/	/	/	/	/	1.0	2.17(3)	0.001
O3	/	/	/	/	/	/	/	/	/	1.0	2.49(2)	0.001
Fe1	/	/	/	1.4	3.28(6)	0.004	1.3	3.27(4)	0.004	1.0	3.28(4)	0.001

Δk: Fourier transformed k-range, ΔR: fit range, ΔE: shift in ionization energy where E is the threshold energy taken as maximum of the first derivative, N: coordination number, R: interatomic distance, σ^2: Debye-Waller term, R_f represents the absolute misfit between the theoretical fitting and the data. Uncertainty estimate is shown in parentheses, otherwise the parameter was held fixed.

containing 1 2 atoms. Fit results agree with reported data of Sher man and Randall for As(V) adsorbed to Fe^{III} (hydr)oxides [48]. These authors applied density functional theory calculations and EXAFS spectroscopy and found that As(V) forms bidentate corner sharing (^{2}C) surface complexes. Consequently, As(V) forms comparable complexes at the surface of SSI. For the sorption sam ple at pH 9.4, additional O contributions at 2.17 and 2.49 Å were required to fit the data. The origin of the presence of these shells is not yet completely clear but tentatively attributed to hydration water molecules of sodium atoms adsorbed in the vicinity of As(V).

Arsenic(V) was also contacted with goethite and with freshly precipitated ferrihydrite in suspension and used as reference compounds (Supplemental Information). For these two samples, fit results comparable to that of the As(V) SSI sorption samples were obtained, further strengthening the idea that similar surface complexes are formed at the surface of all these Fe^{III} (hydr) oxides. In conclusion, this EXAFS study demonstrates the domi nant presence of an As(V) bidentate inner sphere complexes on the SSI surface.

3.4. Surface complexation modelling

The As(V) adsorption gradually but markedly decreases with increasing pH (Fig. 6A, B). Thus, more than 99% of As(V) is adsorbed at pH 4 at an initial As(V) concentration of 1.33 µmol/L, while 60% of As(V) is adsorbed at pH 4 at an initial As(V) concentration of 270 µmol/L in 0.2 g/L SSI suspensions. For higher initial As(V) con centration, the SSI particle surface reached maximum possible adsorption resulting in lower relative As(V) sorption. However, a marked decrease in adsorption with increasing pH is still observed (Fig. 6B).

Relevant As(V) surface complexes are selected according to the above XANES and EXAFS study and further spectroscopic informa tion available for As(V) binding to other Fe^{III} (hydr)oxides (Table 4). Studies of As(V) adsorption on these Fe^{III} (hydr)oxides have shown that inner sphere surface complexes form predominantly with sin gly coordinated surface groups (Table 4). While different As(V) spe cies have been observed for different types of Fe^{III} (hydr)oxides, bidentate species are dominating (Table 4). Together with the bidentate inner sphere complex of As(V) adsorption on SSI inferred from EXAFS, our starting point is that the bidentate As(V) surface complex is the dominant species on the SSI surface. At low pH, this species may be protonated.

$$2\ FeOH^{1/2} + 2H^+ + AsO_4^{3} \leftrightarrow 8\ Fe_2O_2AsO_2^{2} + 2\ H_2O \quad (6)$$

$$2\ FeOH^{1/2} + 3H^+ + AsO_4^{3} \leftrightarrow Fe_2O_2AsO_2H^{1} + 2\ H_2O \quad (7)$$

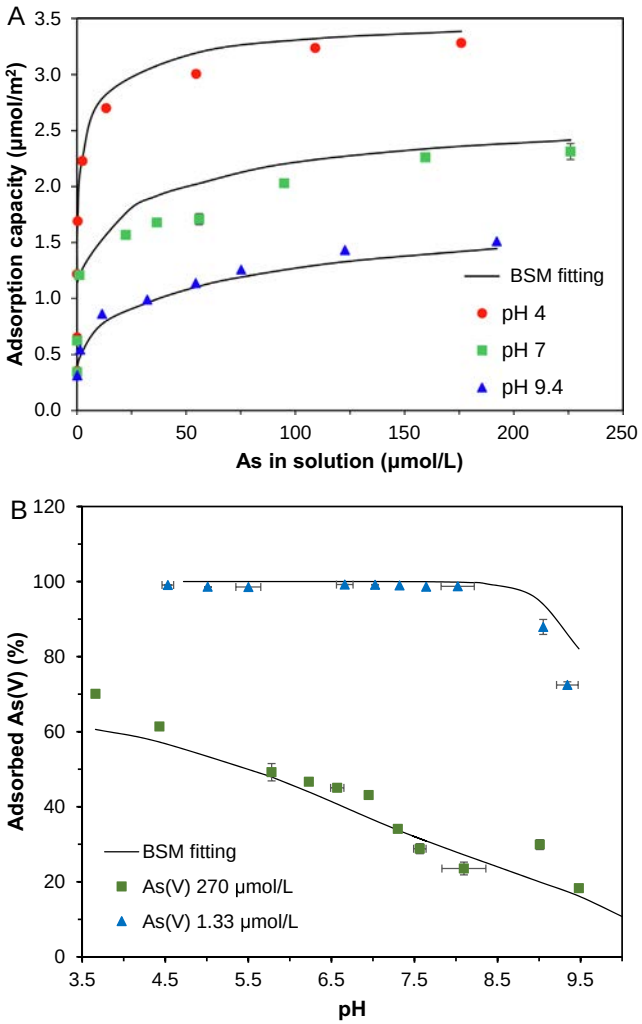

Fig. 6. (A) Adsorption isotherms of As(V) binding to SSI fitted by the 1-pK BSM model assuming bidentate and protonated bidentate As(V) surface complexes only (SSI dose 0.2 g/L, initial As(V) concentration 270 µmol/L, background electrolyte 0.01 mol/L $NaNO_3$). (B) Fraction of total As(V) adsorbed at two concentration levels and at different pH simulated by the 1-pK BSM simulation (initial As(V) concentration 270 µmol/L and 1.33 µmol/L, respectively, SSI dose 0.2 g/L, background electrolyte 0.01 mol/L $NaNO_3$). Error bars represent the difference between each duplicate.

The surface complexation constants are obtained by fitting the adsorption isotherm and adsorption envelope data using the 1 pK BSM. The log K values obtained by Visual MINTEQ [54] for

Table 4
Arsenic(V) surface complexes on Fe^{III}-(hydr)oxides.

Fe^{III}-(hydr)oxides	Analysis	Surface complexation species	Ref
Goethite	EXAFS[a]	Bidentate, Protonated Bidentate	[16]
Hematite	EXAFS	Bidentate, Protonated Bidentate	[61,62]
Goethite, Akaganeite, and Lepidocrocite	EXAFS	Bidentate	[46]
Ferrihydrite	EXAFS	Bidentate and Monodentate	[46,63]

[a] X-ray absorption fine structure spectroscopy.

multidentate surface complexes can be directly compared with the values obtained by ECOSAT or PHREEQC, as discussed by Lützen kirchen *et al.* [60]. The log K values for bidentate and protonated bidentate species derived from the fitting were 27.1 and 31.6, respectively (Table 5). Although the values depend on details like the charge distribution factors or the electrostatic model used, the values in Table 1 for surface complexes of the same stoichiom etry are surprisingly close to each other.

The experimental adsorption isotherms and envelope data are well described by the model (R^2 = 0.98, Fig. 6A, B). Monodentate complexes or outer sphere surface complexes were not considered due to the good fit by protonated and non protonated bidentate inner sphere complexes, and because the EXAFS study did not point to other major species than bidentate As(V) inner sphere sur face complexes.

Overall, the model satisfactorily reproduces acid base potentio metric titration of SSI suspension as well as the adsorption of As (V). Doubly and triply coordinated surface groups are supposed not to bind As(V) in the presence of singly coordinated OH groups. However, due to the unknown local arrangement of the different groups, the involvement of doubly or triply coordinated groups cannot be excluded.

3.5. Arsenic(V) surface speciation versus pH

In the natural environment, As(V) primarily exists in solution as $H_2AsO_4^-$ (pH 2.2 6.9) and as $HAsO_4^{2-}$ (pH 6.9 12.2) [64]. Surface speciation of As(V) on SSI based on our model is presented in Fig. 7 as protonated and non protonated bidentate surface com plexation with SSI. The dominant species within the range pH 3.5 to 9.5 is the deprotonated surface bidentate complex ($\equiv Fe_2O_2AsO_2^{\ 2}$), whereas the amount of the protonated bidentate complex ($\equiv Fe_2O_2AsO_2H^{\ 1}$) becomes abundant at low pH.

Other types of Fe^{III} (hydr)oxides, such as goethite, feroxyhyte and ferrihydrite are also relevant sorbents for As(V). The kinetics of As(V) adsorption onto SSI is rapid, reaching equilibrium within 60 min. In comparison, the reported equilibration times for goethite (50 h) [65], lepidocrocite (7 h) [66], feroxyhyte (4 h) [67] and ferrihydrite (range from 2 to 200 h) [5,68,69] are much longer.

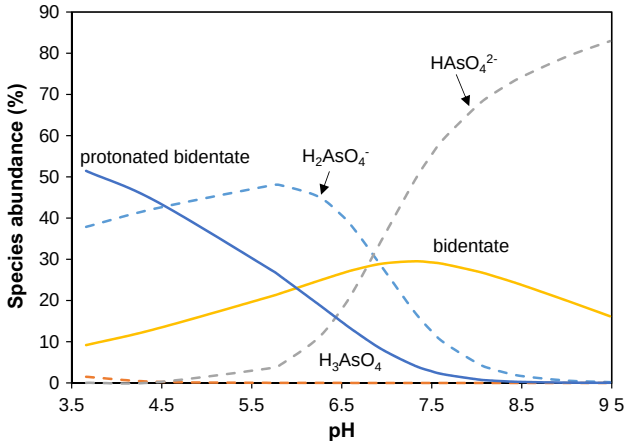

Fig. 7. Predicted As(V) surface speciation on SSI versus pH (solid lines) fitted by the 1-pK BSM model (0.2 g/L SSI, 270 μM As(V)). As(V) speciation in the solution shown for comparison (dashed lines).

The two dimensional morphology and the resulting full exposure of all adsorption sites of the SSI to solution minimize the time for diffusion of As(V) to adsorption sites, which hence reduces the time to reach equilibrium. The maximum observed As(V) uptake on SSI reaches 3.27 μmol/m^2 at pH 4, and 2.3 μmol/m^2 at pH 7. This is higher than the reported maximum adsorption for poorly crystalline goethite (1.33 μmol/m^2; pH 7) [65], similar to lepidocrocite (3.23 μmol/m^2; pH 7) [66], but lower than for ferrihy drite (5.13 μmol/m^2; pH 7) [70] and similar to ultrafine feroxyhyte (3.75 μmol/m^2; pH 7) [67]. However, due to the high specific sur face area of SSI, the maximum sorption uptake per mass is high for SSI compared with any other iron oxide except for ferrihydrite.

The affinity for As(V) bonding to different Fe^{III} (hydr)oxides can be compared based on the surface complexation constants. Using a modelling approach similar to ours (Table 6), Stachowicz *et al.* [18] obtained surface complexation constants for As(V) adsorption on goethite as 26.6, 29.3 and 33.0 for bidentate, protonated bidentate and monodentate surface complexes. Similarly, Gustafsson and Bhattacharya [71] obtained surface complexation constants for As(V) adsorption on ferrihydrite of 27.7 ± 0.7, 34.2 ± 0.3 and 30.7 ± 0.4 for bidentate, protonated bidentate and monodentate surface complexes using the 1 pK TPM CD MUSIC approach. Hence, the surface complexation constants for SSI (27.1 and 31.6) are comparable to those reported for goethite and ferrihydrite (Table 6), suggesting a similarly high binding affinity towards As (V). The differences of surface complexation constants between SSI and other iron Fe^{III} (hydr)oxides are not very large and may be due to variations in the models, i.e. different CD factors, or using a TPM instead of BSM. For further comparison of As(V) affinity to SSI, goethite and ferrihydrite adsorption isotherms are simulated using the 1 pK BSM model (Fig. 8). At intermediate As(V) solution concentrations between 10 and 100 μmol/L a concentration range dominating for model development and optimization the differences in As(V) adsorption to SSI, ferrihydrite and goethite

Table 5
Parameters for the surface complexation reaction of As(V) on SSI in the 1-pK BSM model.

Surface species	Δz_0[a]	Δz_1[b]	Surface complexation reaction on SSI	log K[c]
$\equiv Fe_2O_2AsO_2^{\ 2d}$	0.5	−1.5	$2{\equiv}FeOH^{\ 1/2} + 2H^+ + AsO_4^{\ 3} \leftrightarrow \equiv Fe_2O_2AsO_2^{\ 2} + 2\ H_2O$	27.1
$\equiv Fe_2O_2AsO_2H^{\ 1e}$	0.5	−0.5	$2{\equiv}FeOH^{\ 1/2} + 3H^+ + AsO_4^{\ 3} \leftrightarrow \equiv Fe_2O_2AsO_2H^{\ 1} + 2\ H_2O$	31.6

[a] The charge distribution values at plane 0.
[b] The charge distribution values at plane 1.
[c] The surface complexation constants were derived from 1-pK BSM modelling of the SSI adsorption data.
[d] Bidentate surface complex.
[e] Protonated bidentate surface complex.

Table 6
Comparison of surface complexation parameters for the reaction of As(V) with Fe^{III}-(hydr)oxides.

Solid	PZC	Surface species	C [a]	Δz_0	Δz_1 [b]	Δz_2 [c]	Log K	Ref
Goethite[d]	9.2	Monodentate	0.85 ± 0.01	0.30	−1.30	0	26.6	[18]
		Bidentate		0.47	−1.47	0	29.3	
		Protonated bidentate		0.58	−0.58	0	33	
		Monodentate	1.1	0.25	−2.25	0	20.1	[72]
		Bidentate		0.5	−1.5	0	27.9	
		Protonated bidentate		1.0	−1.0	0	34.5	
Ferrihydrite[d]	8.1	Monodentate	1.1	0.25	−2.25	0	30.7 ± 0.4	[71]
		Bidentate		0.5	−1.5	0	27.7 ± 0.7	
		Protonated bidentate		0.5	−0.5	0	34.2 ± 0.3	
	8.7	Bidentate	0.74	0.47	−1.47	0	27.36 ± 0.07	[73]
		Protonated bidentate		0.58	−0.58	0	31.03 ± 0.45	
SSI	7.8	Bidentate	1.47	0.5	−1.5	–	27.1	This study
		protonated Bidentate		0.5	−0.5	–	31.6	

[a] Inner layer capacitance of Stern layer (F/m^2).
[b] The charge distribution values at Plane 1 in TPM.
[c] The charge distribution values at Plane 2 in TPM.
[d] TPM model was used.

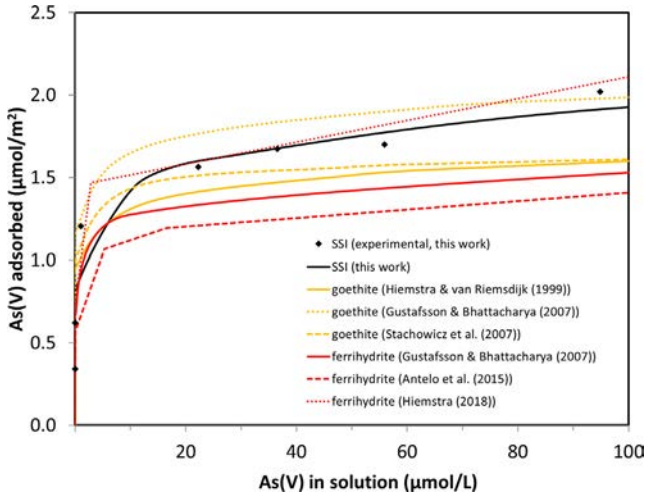

Fig. 8. Comparison of As(V) binding to SSI and other Fe^{III}-(hydr)oxides simulated by 1-pK BSM model using own and published data (solid concentration 0.2 g/L, pH 7, 10 mmol/L $NaNO_3$, 25 °C) [17,71–74].

are small, and differences arising from variable experimental con ditions such as exposure times are likely a cause of larger variation in adsorption than the differences among Fe^{III} (hydr)oxides. At low micromolar to submicromolar As(V) solution concentrations the models are less validated and simulations thus involve larger errors. At a solution concentration of 10 µg/L (0.13 µmol/L), which is equal to the WHO threshold concentration for drinking water, SSI is performing similar to ferrihydrite, while goethites are slightly better based on surface area normalized adsorption. How ever, per mass unit, SSI and ferrihydrite would outcompete goethite due to its lower specific surface area.

4. Conclusions

4.1. Summary of key findings

Batch sorption, acid base titration, XAS and surface complexa tion modelling were used to study the interaction of two dimensional SSI with As(V). XANES spectra showed that the As (V) coordination geometry with SSI was the same between pH 4 and 9 while EXAFS analysis is in agreement with the binding of As(V) as a bidentate inner sphere surface complex. Arsenic(V) sorption was fast, with 90% of final uptake achieved within 10 and 20 min at pH 4 and 7, respectively. The As(V) adsorption was pH dependent, with gradual but marked decrease with increasing pH. Acid base titration and As(V) adsorption data were fitted by the 1 pK BSM. Arsenic(V) adsorption was well described using bidentate surface complexes in the surface complexation model, with stability constants of comparable magnitudes as in previous studies of As(V) sorption to Fe^{III} (hydr)oxides involving similar models.

4.2. Hypothesis, new concepts and innovations

Hypothesis: With an altered brucite layer structure and ultra thin particle thickness, SSI will permit fast and strong bonding of As(V).

New concept/innovation: Ultrathin SSI particles comprising corrugated sheets of Fe O(H) octahedra exhibit a high density of active single coordinated OH sites with fast removal and strong complexation of As(V).

4.3. Summary of key improvements compared to findings in the literature

The rate of As(V) adsorption to SSI was found to be very fast compared with other Fe^{III} (hydr)oxides owing to the high aspect ratio and high BET of SSI. The As(V) surface complexation constants are comparable to those observed for other Fe^{III} (hydr)oxides with similar models. The surface area normalized adsorption capacity of SSI is similar to goethite and ferrihydrite. At micromolar to submi cromolar As(V) solution concentrations, SSI is showing similar binding affinity as ferrihydrite. The advantages of SSI over goethite and ferrihydrite is due to its fast sorption, high specific surface area and its structural stability.

4.4. Vision for future work

The results show that SSI is a promising material for fast and strong adsorption of As(V) from polluted waters at low solution concentrations. SSI may be of interest as a sorbent for other oxyan ions, and for producing composite sorbents e.g. sandwich compos ites with other platy sorbents such as graphene oxide, and for adding further functionalities such as magnetic anchors.

Declaration of Competing Interest

The authors declare no competing financial interest.

Acknowledgments

We acknowledge the KIT Synchrotron Light Source and the Institute for Beam Physics and Technology (IBPT) for the operation of the storage ring, the Karlsruhe Research Accelerator (KARA). We also want to give our gratitude to the financial support of the University of Copenhagen and China Scholarship Council.

References

[1] M.F. Hughes, B.D. Beck, Y. Chen, A.S. Lewis, D.J. Thomas, Arsenic exposure and toxicology: a historical perspective, Toxicol. Sci. 123 (2011) 305–332, https://doi.org/10.1093/toxsci/kfr184.
[2] S. Shankar, U. Shanker, Shikha, Arsenic contamination of groundwater: a review of sources, prevalence, health risks, and strategies for mitigation, Sci. World J. 2014 (2014) 1–18, https://doi.org/10.1155/2014/304524.
[3] World Health Organization, Background document for preparation of WHO Guidelines for drinking-water quality, 2003. doi:WHO/SDE/WSH/03.04/100.
[4] P. Qi, T. Pichler, Closer look at As(III) and As(V) adsorption onto ferrihydrite under competitive conditions, Langmuir 30 (2014) 11110–11116, https://doi.org/10.1021/la502740w.
[5] K.P. Raven, A. Jain, R.H. Loeppert, Arsenite and arsenate adsorption on ferrihydrite : kinetics, equilibrium, and adsorption envelopes, Environ. Sci. Technol. 32 (1998) 344–349, https://doi.org/10.1021/es970421p.
[6] G. Ona-nguema, EXAFS analysis of arsenite adsorption onto two-line ferrihydrite, hematite, goethite, and lepidocrocite, Environ. Sci. Technol. 39 (2005) 9147–9155, https://doi.org/10.1021/es050889p.
[7] C. Mikutta, J. Frommer, A. Voegelin, R. Kaegi, R. Kretzschmar, Effect of citrate on the local Fe coordination in ferrihydrite, arsenate binding, and ternary arsenate complex formation, Geochim. Cosmochim. Acta 74 (2010) 5574–5592, https://doi.org/10.1016/j.gca.2010.06.024.
[8] R. Harrington, D.B. Hausner, N. Bhandari, D.R. Strongin, K.W. Chapman, P.J. Chupas, D.S. Middlemiss, C.P. Grey, J.B. Parise, Investigation of surface structures by powder diffraction : a differential pair distribution function study on arsenate sorption on ferrihydrite, Inorg. Chem. 11 (2010) 325–330, https://doi.org/10.1021/ic9022695.
[9] L. Huo, X. Zeng, S. Su, L. Bai, Y. Wang, Enhanced removal of As (V) from aqueous solution using modified hydrous ferric oxide nanoparticles, Sci. Rep. 7 (2017) 40765, https://doi.org/10.1038/srep40765.
[10] W. Dong, J. Wan, Additive surface complexation modeling of uranium(VI) adsorption onto quartz-sand dominated sediments, Environ. Sci. Technol. 48 (2014) 6569–6577, https://doi.org/10.1021/es501782g.
[11] B.A. Manning, S. Goldberg, Modeling competitive adsorption of arsenate with phosphate and molybdate on oxide minerals, Soil Sci. Soc. Am. J. 60 (1996) 121, https://doi.org/10.2136/sssaj1996.03615995006000010020x.
[12] S. Dixit, J.G. Hering, Comparison of arsenic(V) and arsenic(III) sorption onto iron oxide minerals: implications for arsenic mobility, Environ. Sci. Technol. 37 (2003) 4182–4189, https://doi.org/10.1021/es030309t.
[13] S. Dixit, J.G. Hering, Sorption of Fe(II) and As(III) on goethite in single- and dual-sorbate systems, Chem. Geol. 228 (2006) 6–15, https://doi.org/10.1016/j.chemgeo.2005.11.015.
[14] Y. Gao, A. Mucci, Acid base reactions, phosphate and arsenate complexation, and their competitive adsorption at the surface of goethite in 0.7 M NaCl solution, Geochim. Cosmochim. Acta 65 (2001) 2361–2378, https://doi.org/10.1016/S0016-7037(01)00589-0.
[15] Y. Gao, A. Mucci, Individual and competitive adsorption of phosphate and arsenate on goethite in artificial seawater, Chem. Geol. 199 (2003) 91–109, https://doi.org/10.1016/S0009-2541(03)00119-0.
[16] M. Stachowicz, T. Hiemstra, W.H. van Riemsdijk, Surface speciation of As(III) and As(V) in relation to charge distribution, J. Colloid Interface Sci. 302 (2006) 62–75, https://doi.org/10.1016/j.jcis.2006.06.030.
[17] M. Stachowicz, T. Hiemstra, W.H. van Riemsdijk, Arsenic−bicarbonate interaction on goethite particles, Environ. Sci. Technol. 41 (2007) 5620–5625, https://doi.org/10.1021/es063087i.
[18] M. Stachowicz, T. Hiemstra, W.H. van Riemsdijk, Multi-competitive interaction of As(III) and As(V) oxyanions with Ca^{2+}, Mg^{2+}, PO_4^3 , and CO_3^2 ions on goethite, J. Colloid Interface Sci. 320 (2008) 400–414, https://doi.org/10.1016/j.jcis.2008.01.007.
[19] S.J. Traina, Surface complexation modeling: hydrous ferric oxide, Geochim. Cosmochim. Acta 60 (1996) 4291, https://doi.org/10.1016/S0016-7037(97)81467-6.
[20] M.A. Ali, D.A. Dzombak, Competitive sorption of simple organic acids and sulfate on goethite, Environ. Sci. Technol. 30 (1996) 1061–1071, https://doi.org/10.1021/es940723g.
[21] J. Antelo, S. Fiol, C. Pérez, S. Mariño, F. Arce, D. Gondar, R. López, Analysis of phosphate adsorption onto ferrihydrite using the CD-MUSIC model, J. Colloid Interface Sci. 347 (2010) 112–119, https://doi.org/10.1016/j.jcis.2010.03.020.
[22] M.A. Larsson, I. Persson, C. Sjöstedt, J.P. Gustafsson, Vanadate complexation to ferrihydrite: X-ray absorption spectroscopy and CD-MUSIC modelling, Environ. Chem. 14 (2017) 141–150, https://doi.org/10.1071/en16174.
[23] G.A. Parks, The isoelectric points of solid oxides, solid hydroxides, and aqueous hydroxo complex systems, Chem. Rev. 65 (1965) 177–198, https://doi.org/10.1021/cr60234a002.
[24] J. Lützenkirchen, Comparison of 1-pK and 2-pK versions of surface complexation theory by the goodness of fit in describing surface charge data of (hydr)oxides, Environ. Sci. Technol. 32 (1998) 3149–3154, https://doi.org/10.1021/es980125s.
[25] M. Adachi-Pagano, C. Forano, J.-P. Besse, Delamination of layered double hydroxides by use of surfactants, Chem. Commun. (2000) 91–92, https://doi.org/10.1039/a908251d.
[26] M. Singh, M.I. Ogden, G.M. Parkinson, C.E. Buckley, J. Connolly, Delamination and re-assembly of surfactant-containing Li/Al layered double hydroxides, J. Mater. Chem. 14 (2004) 871–874, https://doi.org/10.1039/b314288d.
[27] R. Ma, Z. Liu, L. Li, N. Iyi, T. Sasaki, Exfoliating layered double hydroxides in formamide: a method to obtain positively charged nanosheets, J. Mater. Chem. 16 (2006) 3809–3813, https://doi.org/10.1039/b605422f.
[28] T. Hibino, W. Jones, New approach to the delamination of layered double hydroxides, J. Mater. Chem. 11 (2001) 1321–1323, https://doi.org/10.1039/b101135i.
[29] B. Hudcová, V. Veselská, J. Filip, S. Číhalová, M. Komárek, Sorption mechanisms of arsenate on Mg-Fe layered double hydroxides: A combination of adsorption modeling and solid state analysis, Chemosphere 168 (2017) 539–548, https://doi.org/10.1016/j.chemosphere.2016.11.031.
[30] Y. You, G.F. Vance, H. Zhao, Selenium adsorption on Mg–Al and Zn–Al layered double hydroxides, Appl. Clay Sci. 20 (2001) 13–25, https://doi.org/10.1016/S0169-1317(00)00043-0.
[31] L. Huang, L. Fang, T. Hassenkam, K.N. Dalby, K.G. Scheckel, H.C.B. Hansen, A one-step delamination procedure to form single sheet iron(iii)-(oxy) hydroxides, J. Mater. Chem. A 1 (2013) 13664, https://doi.org/10.1039/c3ta12495a.
[32] L. Fang, L. Huang, P.E. Holm, X. Yang, H.C.B. Hansen, D. Wang, Facile upscaled synthesis of layered iron oxide nanosheets and their application in phosphate removal, J. Mater. Chem. A 3 (2015) 7505–7512, https://doi.org/10.1039/C4TA07083F.
[33] Z. Yin, K. Dideriksen, M. Abdelmoula, C. Ruby, F.M. Michel, M.J. Bjerrum, H.C.B. Hansen, Structure of single sheet iron oxides produced from surfactant interlayered green rusts, Appl. Clay Sci. 170 (2019) 86–96, https://doi.org/10.1016/j.clay.2019.01.009.
[34] S. Brunauer, P.H. Emmett, E. Teller, Adsorption of gases in multimolecular layers, J. Am. Chem. Soc. 60 (1938) 309–319, https://doi.org/10.1021/ja01269a023.
[35] J. Lützenkirchen, T. Preočanin, D. Kovačević, V. Tomišić, L. Lövgren, N. Kallay, Potentiometric titrations as a tool for surface charge determination, Croat. Chem. Acta 85 (2012) 391–417, https://doi.org/10.5562/cca2062.
[36] Y. Ho, G. McKay, Pseudo-second order model for sorption processes, Process Biochem. 34 (1999) 451–465, https://doi.org/10.1016/S0032-9592(98)00112-5.
[37] J. Rothe, S. Butorin, K. Dardenne, M.A. Denecke, B. Kienzler, M. Löble, V. Metz, A. Seibert, M. Steppert, T. Vitova, C. Walther, H. Geckeis, The INE-Beamline for actinide science at ANKA 043105, Rev. Sci. Instrum. 83 (2012), https://doi.org/10.1063/1.3700813.
[38] B. Ravel, M. Newville, ATHENA, ARTEMIS, HEPHAESTUS : data analysis for X-ray absorption spectroscopy using IFEFFIT, J. Synchrotron Radiat. 12 (2005) 537–541, https://doi.org/10.1107/S0909049505012719.
[39] A.L. Ankudinov, B. Ravel, J.J. Rehr, S.D. Conradson, Real-space multiple-scattering calculation and interpretation of x-ray-absorption near-edge structure, Phys. Rev. B 58 (1998) 7565–7576, https://doi.org/10.1103/PhysRevB.58.7565.
[40] J. Lützenkirchen, J.F. Boily, L. Gunneriusson, L. Lövgren, S. Sjöberg, Protonation of different goethite surfaces—unified models for $NaNO_3$ and NaCl media, J. Colloid Interface Sci. 317 (2008) 155–165, https://doi.org/10.1016/j.jcis.2007.08.055.
[41] E.M. Moon, C.L. Peacock, Modelling Cu(II) adsorption to ferrihydrite and ferrihydrite–bacteria composites: Deviation from additive adsorption in the composite sorption system, Geochim. Cosmochim. Acta 104 (2013) 148–164, https://doi.org/10.1016/j.gca.2012.11.030.
[42] J.C.W. A.L. Herbelin, FITEQL 4.0: a computer program for determination of chemical equilibrium constants from experimental data, 1999.
[43] E.P. Poeter, M.C. Hill, UCODE, a computer code for universal inverse modeling, Comput. Geosci. 25 (1999) 457–462, https://doi.org/10.1016/S0098-3004(98)00149-6.
[44] T. Hiemstra, W.H. Van Riemsdijk, A surface structural approach to ion adsorption: the charge distribution (CD) model, J. Colloid Interface Sci. 179 (1996) 488–508, https://doi.org/10.1006/jcis.1996.0242.
[45] C.J. Tadanier, M.J. Eick, Formulating the charge-distribution multisite surface complexation model using FITEQL, Soil Sci. Soc. Am. J. 66 (2002) 1505, https://doi.org/10.2136/sssaj2002.1505.
[46] G. Waychunas, B. Rea, C. Fuller, J. Davis, Surface chemistry of ferrihydrite: Part 1. EXAFS studies of the geometry of coprecipitated and adsorbed arsenate,

Geochim. Cosmochim. Acta 57 (1993) 2251–2269, https://doi.org/10.1016/0016-7037(93)90567-G.
[47] S. Fendorf, M.J. Eick, P. Grossl, D.L. Sparks, Arsenate and chromate retention mechanisms on goethite. 1. Surface structure, Environ. Sci. Technol. 31 (1997) 315–320, https://doi.org/10.1021/es950653t.
[48] D.M. Sherman, S.R. Randall, Surface complexation of arsenic(V) to iron(III) (hydr)oxides: structural mechanism from ab initio molecular geometries and EXAFS spectroscopy, Geochim. Cosmochim. Acta 67 (2003) 4223–4230, https://doi.org/10.1016/S0016-7037(03)00237-0.
[49] T. Hiemstra, W.H. Van Riemsdijk, A surface structural model for ferrihydrite I: Sites related to primary charge, molar mass, and mass density, Geochim. Cosmochim. Acta 73 (2009) 4423–4436, https://doi.org/10.1016/j.gca.2009.04.032.
[50] L. Spadini, A. Manceau, P.W. Schindler, L. Charlet, Structure and stability of Cd^{2+} surface complexes on ferric oxides, J. Colloid Interface Sci. 168 (1994) 73–86, https://doi.org/10.1006/jcis.1994.1395.
[51] J.S. Loring, M.H. Sandström, K. Norén, P. Persson, Rethinking arsenate coordination at the surface of goethite, Chem. - A Eur. J. 15 (2009) 5063–5072, https://doi.org/10.1002/chem.200900284.
[52] J. Lützenkirchen, F. Heberling, F. Supljika, T. Preocanin, N. Kallay, F. Johann, L. Weisser, P.J. Eng, Structure–charge relationship – the case of hematite (001), Faraday Discuss. 180 (2015) 55–79, https://doi.org/10.1039/C4FD00260A.
[53] L. Stolze, D. Zhang, H. Guo, M. Rolle, Surface complexation modeling of arsenic mobilization from goethite: Interpretation of an in-situ experiment, Geochim. Cosmochim. Acta 248 (2019) 274–288, https://doi.org/10.1016/j.gca.2019.01.008.
[54] J.P. Gustafsson, Visual MINTEQ, Version 3.1, KTH, Stock. Sweden. 5 (2013) http://vminteq.lwr.kth.se/download/.
[55] J. Doherty, PEST: a unique computer program for model-independent parameter optimisation, in: Water Down Under 94 Groundwater/Surface Hydrol. Common Interes. Pap. Prepr. Pap., 1994, pp. 551. http://search.informit.com.au/documentSummary;dn=752715546665009;res=IELENG.
[56] J. Lützenkirchen, A. Abdelmonem, R. Weerasooriya, F. Heberling, V. Metz, R. Marsac, Adsorption of dissolved aluminum on sapphire-c and kaolinite: implications for points of zero charge of clay minerals, Geochem. Trans. 15 (2014) 9, https://doi.org/10.1186/1467-4866-15-9.
[57] M.V. Fedorov, A.A. Kornyshev, Towards understanding the structure and capacitance of electrical double layer in ionic liquids, Electrochim. Acta 53 (2008) 6835–6840, https://doi.org/10.1016/j.electacta.2008.02.065.
[58] K.D. Zur Loye, A.M. Latshaw, M.D. Smith, W.M. Chance, H.-C. Zur Loye, Synthesis and crystal structure of sodium arsenate oxyhydroxide: $Na_4(AsO_4)OH$, J. Chem. Crystallogr. 45 (2015) 20–25, https://doi.org/10.1007/s10870-014-0558-7.
[59] Y. Arai, E.J. Elzinga, D.L. Sparks, X-ray absorption spectroscopic investigation of arsenite and arsenate adsorption at the aluminum oxide–water interface, J. Colloid Interface Sci. 235 (2001) 80–88, https://doi.org/10.1006/jcis.2000.7249.
[60] J. Lützenkirchen, R. Marsac, D.A. Kulik, T.E. Payne, Z. Xue, S. Orsetti, S.B. Haderlein, Treatment of multi-dentate surface complexes and diffuse layer implementation in various speciation codes, Appl. Geochem. 55 (2015) 128–137, https://doi.org/10.1016/j.apgeochem.2014.07.006.
[61] J.G. Catalano, Z. Zhang, C. Park, P. Fenter, M.J. Bedzyk, Bridging arsenate surface complexes on the hematite (012) surface, Geochim. Cosmochim. Acta 71 (2007) 1883–1897, https://doi.org/10.1016/j.gca.2007.01.015.
[62] G. Waychunas, T. Trainor, P. Eng, J. Catalano, G. Brown, J. Davis, J. Rogers, J. Bargar, Surface complexation studied via combined grazing-incidence EXAFS and surface diffraction: arsenate on hematite (0001) and (10–12), Anal. Bioanal. Chem. 383 (2005) 12–27, https://doi.org/10.1007/s00216-005-3393-z.
[63] T. Hiemstra, W. Zhao, Reactivity of ferrihydrite and ferritin in relation to surface structure, size, and nanoparticle formation studied for phosphate and arsenate, Environ. Sci. Nano. 3 (2016) 1265–1279, https://doi.org/10.1039/C6EN00061D.
[64] A.H. Welch, K.G. Stollenwerk, Arsenic in Ground Water, Springer, US, Boston MA, 2003. doi:10.1007/b101867.
[65] J. Gimenez, M. Martinez, J. Depablo, M. Rovira, L. Duro, Arsenic sorption onto natural hematite, magnetite, and goethite, J. Hazard. Mater. 141 (2007) 575–580, https://doi.org/10.1016/j.jhazmat.2006.07.020.
[66] E. Repo, M. Mäkinen, S. Rengaraj, G. Natarajan, A. Bhatnagar, M. Sillanpää, Lepidocrocite and its heat-treated forms as effective arsenic adsorbents in aqueous medium, Chem. Eng. J. 180 (2012) 159–169, https://doi.org/10.1016/j.cej.2011.11.030.
[67] M.C.S. Faria, R.S. Rosemberg, C.A. Bomfeti, D.S. Monteiro, F. Barbosa, L.C.A. Oliveira, M. Rodriguez, M.C. Pereira, J.L. Rodrigues, Arsenic removal from contaminated water by ultrafine δ-FeOOH adsorbents, Chem. Eng. J. 237 (2014) 47–54, https://doi.org/10.1016/j.cej.2013.10.006.
[68] C.C. Fuller, J.A. Davis, G.A. Waychunas, Surface chemistry of ferrihydrite: Part 2. Kinetics of arsenate adsorption and coprecipitation, Geochim. Cosmochim. Acta 57 (1993) 2271–2282, https://doi.org/10.1016/0016-7037(93)90568-H.
[69] P.J. Swedlund, H. Holtkamp, Y. Song, C.J. Daughney, Arsenate–ferrihydrite systems from minutes to months: a macroscopic and IR spectroscopic study of an elusive equilibrium, Environ. Sci. Technol. 48 (2014) 2759–2765, https://doi.org/10.1021/es404742c.
[70] W.R. Richmond, M. Loan, J. Morton, G.M. Parkinson, A.J.P. Crc, Arsenic removal from aqueous solution via ferrihydrite crystallization control, Environ. Sci. Technol. 38 (2004) 2368–2372, https://doi.org/10.1021/es0353154.
[71] J.P. Gustafsson, P. Bhattacharya, Geochemical modelling of arsenic adsorption to oxide surfaces, Trace Met. Other Contam. Environ. (2007) 159–206, https://doi.org/10.1016/S1875-1121(06)09006-7.
[72] T. Hiemstra, W.H. Van Riemsdijk, Surface structural ion adsorption modeling of competitive binding of oxyanions by metal (hydr)oxides, J. Colloid Interface Sci. 210 (1999) 182–193, https://doi.org/10.1006/jcis.1998.5904.
[73] J. Antelo, F. Arce, S. Fiol, Arsenate and phosphate adsorption on ferrihydrite nanoparticles. Synergetic interaction with calcium ions, Chem. Geol. 410 (2015) 53–62, https://doi.org/10.1016/j.chemgeo.2015.06.011.
[74] T. Hiemstra, Ferrihydrite interaction with silicate and competing oxyanions: geometry and hydrogen bonding of surface species, Geochim. Cosmochim. Acta 238 (2018) 453–476, https://doi.org/10.1016/j.gca.2018.07.017.